2022

Influence of Foundation Damping on Offshore Wind Turbine Monopile Design Loads

Wystan Carswell
University of Massachusetts Amherst

Sanjay R. Arwade
University of Massachusetts Amherst

Jörgen Johansson
Norwegian Geotechnical Institute

Don J. DeGroot
University of Massachusetts Amherst

Carswell, Wystan; Arwade, Sanjay R.; Johansson, Jörgen; and DeGroot, Don J., "Influence of Foundation Damping on Offshore Wind Turbine Monopile Design Loads" (2022). *Marine Structures*. 13.
https://doi.org/10.1016/j.marstruc.2021.103154

Influence of Foundation Damping on Offshore Wind Turbine Monopile Design Loads

Modeling hysteretic material damping from soil-foundation interaction

Wystan Carswell[1]**,** Haley & Aldrich, Inc., University of Massachusetts Amherst
Sanjay R. Arwade, University of Massachusetts Amherst
Jörgen Johansson, Norwegian Geotechnical Institute
Don J. DeGroot, University of Massachusetts Amherst

Abstract

The dynamic behavior of offshore wind turbines (OWTs) must be designed considering stochastic load amplitudes and frequencies from waves and mechanical loads associated with the spinning rotor during power production. The proximity of the OWT natural frequency to excitation frequencies combined with low damping necessitates a thorough analysis of sources of damping; of these sources of damping, least is known about the contributions of damping from soil-structure interaction (foundation damping). This paper studies the influence of foundation damping on cyclic load demand for monopile-supported OWTs considering the design situations of power production, emergency shutdown, and parked conditions. The NREL 5MW Reference Turbine was modeled using the aero-hydro-elastic software FAST and included equivalent linear foundation stiffness and damping matrices. These matrices were determined using an iterative approach with FAST mudline loads as input to a soil-pile finite element software which calculates hysteretic material damping. Accounting for foundation damping in time history analysis can reduce cyclic foundation moment demand by as much as 30% during parked conditions, 25-33% during emergency shutdown, but only 2-3% reduction during power production without wave and wind misalignment. The calculated foundation damping from the emergency shutdown cases agreed with experimental testing performed in similar site conditions.

[1] Corresponding author.
e. wcarswell@haleyaldrich.com
t. +1 617-886-7357
465 Medford Street, Suite 2200, Boston, Massachusetts 02129

Nomenclature

DE	Delaware
DLC	Design load case
DNV	Det Norske Veritas
ESS	Extreme Sea State
ETM	Extreme Turbulence Model
EWH	Extreme Wave Height
EWM	Extreme Wind Model
EWS	Extreme Wind Shear
HSS	High-speed shaft
IEC	International Electrotechnical Commission
NGI	Norwegian Geotechnical Institute
NOAA	National Ocean and Atmospheric Administration
NREL	National Renewable Energy Laboratory
NSS	Normal Sea State
NTM	Normal Turbulence Model
OWT	Offshore wind turbine
RWH	Reduced Wave Height
RWM	Reduced Wind Model
SSS	Severe Sea State
SWH	Severe Wave Height
TI	Turbulence intensity
ULS	Ultimate limit state
c_{mud}	Mudline damping matrix
$c_{\phi\phi}$	Mudline rotational dashpot
f	Natural frequency
g	Acceleration due to gravity
k_{mud}	Mudline stiffness matrix
k_{xx}, k_{yy}	Horizontal translational stiffness
$k_{x\phi}$	Coupled stiffness term
$k_{\phi\phi}$	Rotational stiffness
s_u	Undrained shear strength
u	Cyclic amplitude of mudline displacement
v_{in}, v_{rated}, v_{out}	Cut-in, rated, cut-out wind speed
x	Horizontal degree of freedom in fore-aft direction
y	Horizontal degree of freedom in side-to-side direction
z	Vertical degree of freedom
E	Modulus of elasticity
E_h	Hysteretic energy loss
$E[\cdot]$	Expected value
G_0	Shear modulus at small strains
H	Wave height
H_s	Significant wave height
$H_{N\text{-}yr}$	N-year wave height
F_x	Cyclic amplitude of horizontal mudline force
M_ϕ	Cyclic amplitude of mudline moment
T_p	Peak spectral period
$U_{10,hub}$	10-minute hub height wind speed
U_{hub}	Hub height wind speed
ϕ	Rotational degree of freedom
θ	Cyclic amplitude of mudline rotation
ν	Poisson's ratio
ρ	Density

σ	Standard deviation
ψ	Wave height reduction factor

1 Introduction

Approximately 15-20% of the capital cost of offshore wind farms can be attributed to the foundation and support structure of offshore wind turbines (OWTs) [1–4]. OWT support structures are lightly damped and must withstand highly uncertain offshore wind and wave loads with stochastic load frequency and amplitude in addition to stochastic mechanical loads associated with the spinning rotor during power production. OWTs are typically designed in a so-called "soft-stiff" frequency design regime, wherein the first natural frequency is designed to lie between the 1P and 3P blade rotation frequency bands. Because a stiffer structure implies higher costs (due to increased structural material requirements), it is desirable for the first natural frequency to be near, but safely above the 1P frequency band (DNV suggests a clearance of ±10% of blade rotation frequency bands [5]). The close proximity to excitation frequencies combined with the low amount of damping present in the support structure necessitates a thorough analysis of not only the stiffness, but also the various sources of damping within the OWT system: structural, hydrodynamic, aerodynamic, soil-foundation interaction (foundation), and sometimes tuned mass damper. More damping reduces structural demand, and therefore the material costs.

DNV (2014) recommends soil damping to be considered in the design phase, but no recommended practice for estimating soil damping is suggested; therefore, foundation damping is typically included in the overall structural Rayleigh damping in OWT design [5–7]. While geotechnical finite element models are the most realistic way of assessing foundation damping, they are computationally expensive for structural time history analysis [8]; consequently, other (simplified, less time consuming) ways of including foundation damping in OWT design include the use of a dashpot [9] or by using a macro-element which uses kinematic hardening [10].

Foundation damping is probably the least understood and most complex of all the sources contributing to the OWT system damping, and there is no consensus on its importance in an OWT design context with respect to the other sources of damping [6,11–13]. Previous work [6] indicated that for a monopile-supported OWT subjected to extreme storm loads, cyclic design loads for the pile foundation can be reduced by as much as 10% when foundation damping is incorporated into OWT modeling.

Because over 80% of installed OWTs are supported by monopile foundations [14], this paper evaluates the relative impact of hysteretic foundation damping on monopile foundation loads for power production, emergency stop, and parked storm conditions. The purpose of the paper is not to propose a specific methodology, rather its intention was to better understand how foundation damping affects foundation loads. The methodology for accounting for foundation damping continues to develop and the intention of the paper is to show potential for foundation load reduction for various load cases and not to identify specific reduction quantities (which may vary based on subsurface conditions, metocean conditions, as well as turbine model and size). While studies have shown that radiation damping is small for frequencies below 1 Hz [11,12,15] further research is needed to understand how radiation damping contributes to the foundation damping. This paper, however, only considers the contribution of hysteretic material damping from pile-soil interaction.

The NREL 5MW Reference Turbine ("NREL 5MW") [16] was analyzed using the open-source aeroelastic simulation program FAST (v7, [17]), considering the IEC 61400-3 design load cases (DLCs) [18] to dictate wind, wave, and turbine conditions. Soil-structure interaction was modeled in FAST via mudline stiffness and damping matrices which were calculated using the results from the soil-pile software INFIDEL (INFInite Domain Elements) [19,20]. The NREL 5MW was analyzed considering a North Sea site described by [6] and due to the lack of available metocean data for that location, the approximately equivalent environmental site conditions from the National Ocean and Atmospheric Administration (NOAA) buoy sited off the coast of Delaware in the U.S. Atlantic Ocean were used to determine input wave heights and wind speeds for the DLCs.

Section 2 illustrates the analysis process used to determine the influence of foundation damping on cyclic mudline demand, with further discussion of how foundation stiffness and damping matrices were calculated. Section 3 describes the OWT model used to determine monopile loads and the calculation of foundation stiffness. The DLCs selected for analysis, and how each design situation (power production, emergency shutdown, and parked) was modeled in FAST (Figure 1) is described in Section 4. The results are given in Section 5 and a summary and conclusions in Section 6.

2 Methodology

2.1 Offshore Wind Turbine Analysis Procedure

Several different methods and numerical tools are used in the analysis process of this paper (Figure 1) to define the impact of foundation damping on cyclic foundation demand. The approach described is not recommended as a methodology for design per se, but as an ad hoc approach for evaluating the importance of foundation damping for OWTs in various design situations. Each Design Load Case (DLC, described in Section 4) was initially analyzed using the aeroelastic offshore wind turbine simulation code FAST [17] (further described in Section 4.4) assuming a fixed connection of the substructure at the mudline to estimate cyclic foundation load demand. The cyclic foundation demand was then used as input to INFIDEL [19] (described below) to compute the foundation response (displacement, rotation, and hysteretic energy loss, described in Section 2.2) and the corresponding equivalent linear foundation stiffness and damping matrices. Given the mudline stiffness matrix, new tower mode shapes and frequencies were calculated using the NREL-distributed program BModes [21] and the FAST analysis was repeated with foundation stiffness and damping matrices. Two versions of the OWT model were analyzed for each DLC, one version including the mudline dashpot ("DAMPED" in Figure 1) and one without ("UNDAMPED"), to determine the amplitude of cyclic mudline loads, displacements, and rotations. The impact of foundation damping was assessed by the difference in cyclic foundation demand between the undamped and damped models.

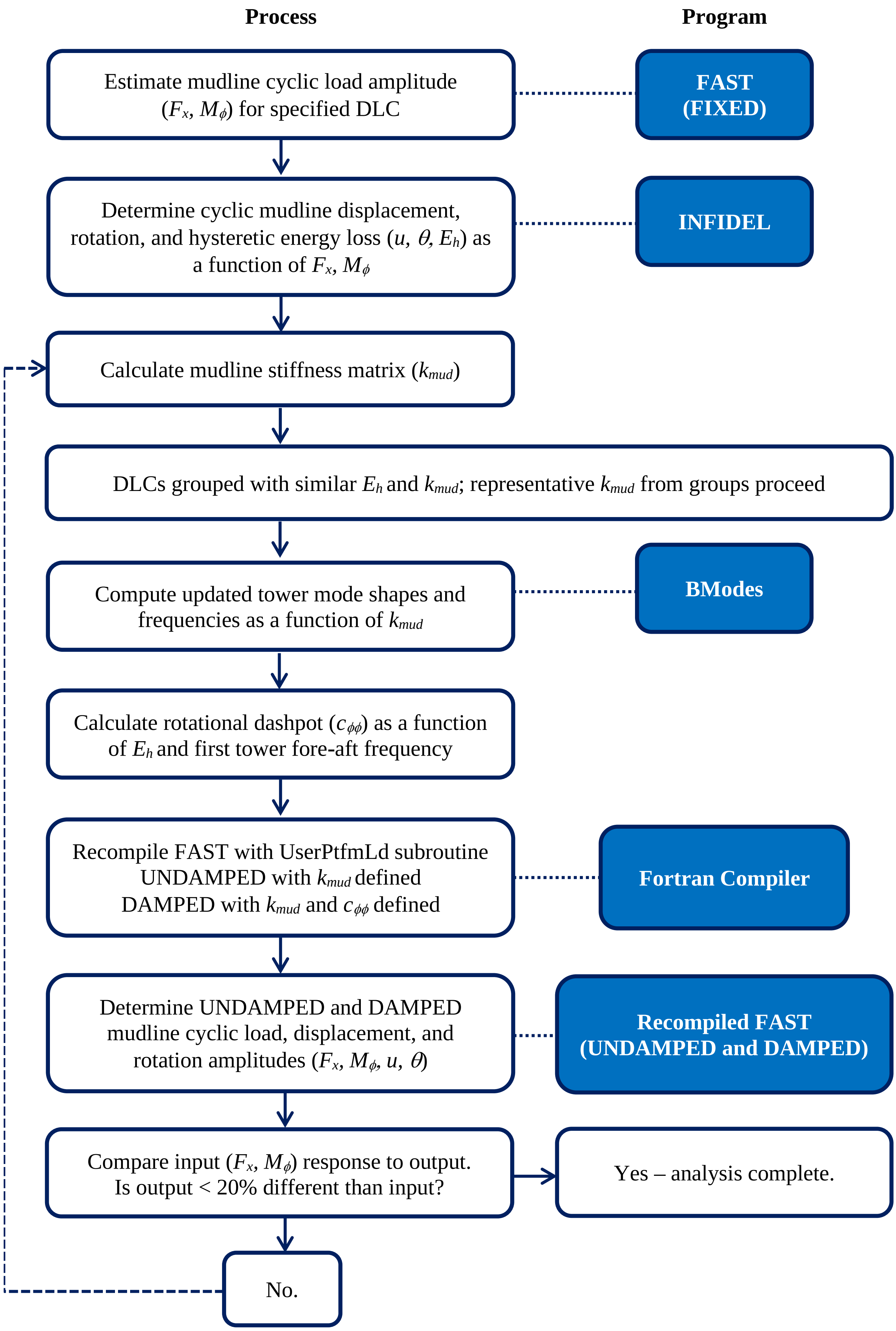

152

153 **Figure 1 Flowchart of foundation damping analysis process**

Because the analysis process (Figure 1) used to define the impact of foundation damping on cyclic OWT monopile design loads is relatively time-consuming, the DLCs were grouped according to similar hysteretic energy loss and mudline stiffness matrices. If the mudline cyclic load amplitudes from the fixed-base FAST analysis and the flexible-base FAST analysis differed by more than 20%, the mudline stiffness matrix was updated and the flexible-base FAST analysis was repeated to ensure the soil-pile properties were approximately compatible with the cyclic load amplitude. The 20% difference in foundation response was chosen as rational ad-hoc criteria, giving an error in the foundation stiffness smaller than 20% (for the purposes of design, it is recommended that the difference in foundation response be less than 20%; inclusion of foundation flexibility in the initial run would reduce iterations). The average difference in response after the first iteration (using fixed-base mudline response to estimate mudline stiffness parameters) was approximately 11%; for cases which exceeded the 20% criteria, a second iteration decreased the average difference in response to approximately 1%. It should be noted that for load cases which use random seeding, the variation in mudline response based on seeding alone can be at least 3%. The resulting small error in eigenfrequency using the criteria cited above was considered negligible for our analysis (it should be noted that the natural frequency from the representative mudline stiffness matrices was on average 0.23 Hz and varied by less than 0.01 Hz). The relative change in natural frequency can be seen in one example time history of tower top displacement (stochastic load case DLC 6.1a, refer to Section 4 and Figure 2A), where there is a significant phase and amplitude difference between the fixed base and first iteration flexible foundation case; with a second iteration, the difference in frequency and amplitude is substantially minimized. Methodology for the analysis herein relied on differences in foundation response: the difference in cyclic mudline moment amplitude from the fixed base to flexible base case was 39% but differed by only 2% after the second iteration (Figure 2B).

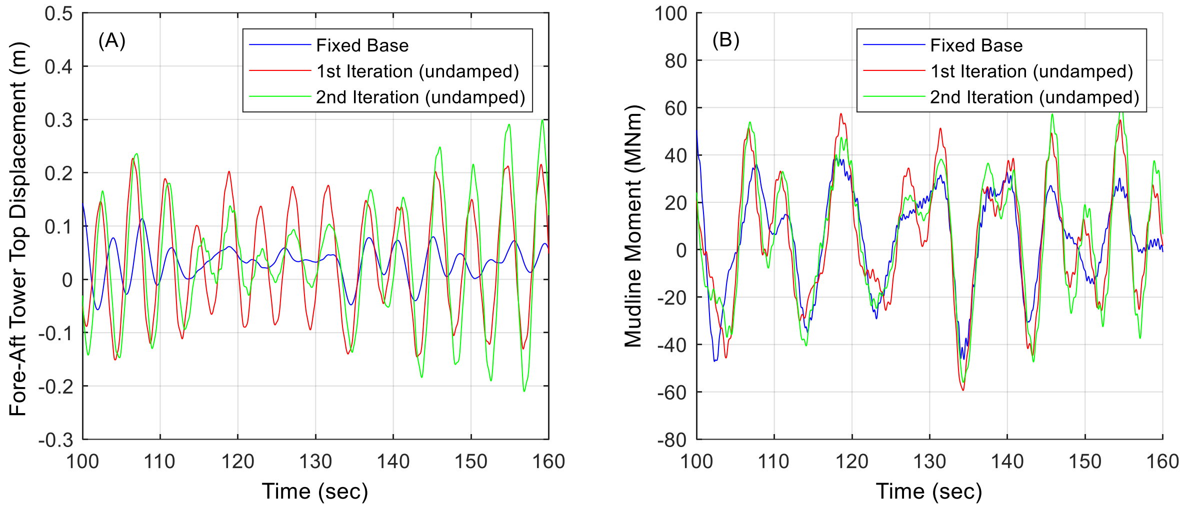

Figure 2 Effect of methodology iteration on (A) tower top displacement and (B) mudline response

In a proper design, further iteration would be required to reduce the difference in mudline response.

The aero-hydro-elastic simulation code FAST uses Blade Element Momentum (BEM) theory to calculate wind loads on OWT blades and includes the effects of the spinning rotor on the support structure dynamics. Time histories of the dynamic behavior of the support structure is computed by superposition of the first and second fore-aft and side-to-side mode shapes. These mode shapes were determined using the NREL-distributed software BModes and are defined by sixth-order polynomial coefficients in the FAST tower property file.

Depending on the requirements of the DLC, wind can be defined as either steady or turbulent and waves as regular or irregular. Turbulent wind conditions were modeled in FAST using the Kaimal spectrum. Linear wave theory was used to generate wave conditions using the JONSWAP spectrum and Wheeler stretching. The effects of breaking waves were neglected.

2.2 Cyclic Load Amplitude for Computing Foundation Stiffness and Damping

Figure 3 show examples of a periodic and stochastic time histories of foundation moment loading. The loading can be visualized as a harmonic loading with an average component and a cyclic amplitude component [22]. The definition of the cyclic amplitude influences the calculations of stiffness and damping – higher cyclic amplitudes lead to higher damping but lower stiffness.

The behavior of cyclically loaded clays is intricate, e.g. the stiffness is more influenced by cyclic load amplitude and number of cycles rather than maximum response [23], as long as the maximum response is much lower than the response corresponding to the ultimate capacity. The ultimate peak load a foundation can sustain is affected by the preceding cyclic loading; thus in an ultimate state load case, the cyclic load amplitude has to be accounted for in addition to the peak load. The cyclic stiffness of soil is also affected by the average load component and there are methods developed to account for this (e.g. [23,24]). While there are procedures for establishing cyclic stress-strain curves accounting for the average load components, more research is needed to understand the effect of average load components and number of load cycles on soil material damping [25].

For regular wave train and steady wind DLCs, estimating cyclic load amplitude was straightforward (due to the periodic nature of the time history output, half of the difference between maximum and minimum response, Figure 3A); for stochastic time histories (with irregular wave trains or turbulent wind fields), these loads were estimated as three times the standard deviation of the response (3σ, Figure 3B [6]). Using three times the standard deviation can be partially justified by the fact that the average load component was not considered (shown with red solid lines Figure 3) which would decrease the foundation stiffness, and the objective of the paper was to understand the order of magnitude of foundation damping has on the foundation loads. In practice, the cyclic and average load amplitude variation in a time history is determined by load cycle counting [26] to estimate the soil degradation and corresponding foundation stiffness and damping.

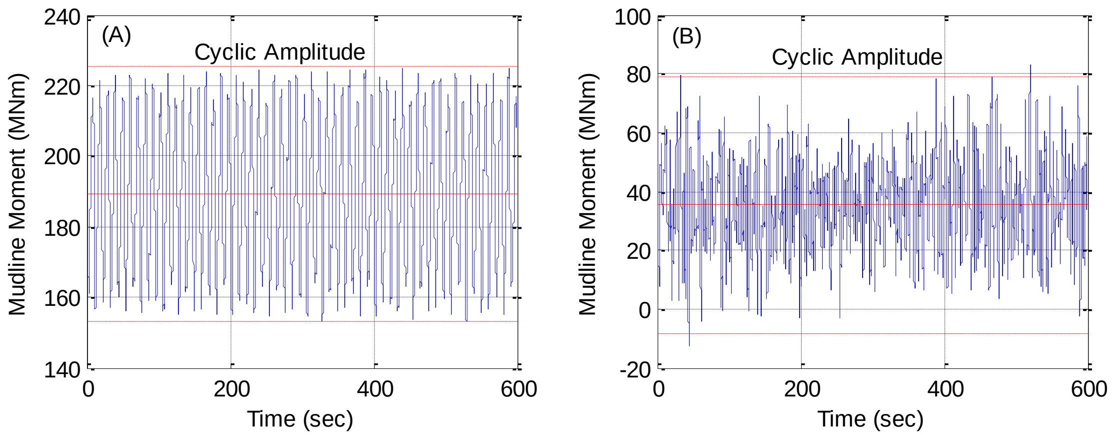

Figure 3 Example time histories indicating load amplitude for (A) regular wave train/steady wind (DLCs 1.5, 6.1c, 6.2b) and (B) stochastic time histories of mudline moment (DLCs 1.1, 1.3, 1.6a, 1.6b, 6.1a, 6.2a)

The emergency shutdown design situation required a somewhat different approach due to the nonstationary nature of the response. In this case, the cyclic amplitude of concern was taken to be the difference between the mean pre-shutdown response and the absolute minimum response (Figure 4). Using mudline stiffness and damping parameters determined for the shutdown cyclic amplitude also for the pre-shutdown portion of the analysis is assumed to have limited influence on our results. Using the maximum amplitude in the beginning of the shutdown process likely overestimates the foundation damping to some extent. Since the focus was to evaluate the effect of damping on the maximum mudline moment occurring at shutdown, it was chosen as simple approach to obtain a first order estimate of foundation damping. Further refinement of the foundation damping estimates is recommended in a real design.

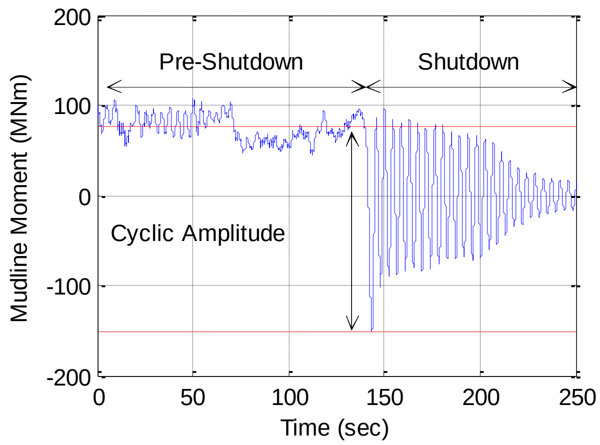

Figure 4 Example emergency shutdown time history of mudline moment during rated wind speeds (DLC 5.1)

2.3 Foundation Stiffness and Damping

The NGI-developed INFIDEL software has been used to compute foundation stiffness and damping matrices for use with FAST [6,19,20]. To the authors' knowledge INFIDEL is the only finite element code which can account for the variation of soil damping with the shear strain distribution around the pile and integrate it to a foundation damping value. The method of computation is very efficient, making it practical for offshore wind turbine design where very many load cases with different load combinations between moment, horizontal and vertical load need to be analyzed. INFIDEL defines an axisymmetric three-dimensional soil-pile space with infinite extents. It models cyclic soil behavior with a nonlinear constitutive model based on user defined stress-strain curves and soil damping curves [27]. The INFIDEL soil-foundation analysis is an equivalent linear approach based on monotonic stress-strain curve which represents the cyclic stress-strain response of the soil. For each load level an equivalent cyclic strain is computed which gives the stress and the damping in each soil element. The software is not iterative and does not include kinematic hardening. Linear elastic pile behavior was assumed. Figure 6 shows the input shear modulus at small strains G_0, undrained shear strength s_u, and Poisson's ratio ν used in the INFIDEL model. The Poisson's ratio for the pile was 0.3. The soil-pile model and methodology of INFIDEL are described in detail by Carswell et al.[6].

The cyclic foundation load amplitudes (H, M) from FAST were used as input to INFIDEL to obtain mudline displacement u and rotation θ. In order to compute the equivalent linear stiffness elements (k_{xx}, $k_{x\phi}$, $k_{\phi\phi}$) comprising k_{mud}, accounting for soil non-linearity, two runs of INFIDEL were required:

1) Using cyclic mudline load amplitudes H and M (denoted $F_{x,1}$ and $M_{\phi,1}$ in Eq. 2) to obtain cyclic mudline displacement and rotation amplitudes u and θ (denoted u_1 and θ_1 in Eq. 2), and
2) Using just the horizontal mudline shear amplitude H ($F_{x,2}$ in Eq. 2) but setting M = 0 to obtain a second set of displacement and rotation amplitudes (u_2 and θ_2).

The displacement and rotation results were then used in conjunction with the input loads to determine k_{mud}, calculated per Zaaijer [28] using

$$\begin{pmatrix} k_{xx} \\ k_{x\varphi} \\ k_{\varphi\varphi} \end{pmatrix} = \begin{pmatrix} u_1 & \theta_1 & 0 \\ 0 & u_1 & \theta_1 \\ u_2 & \theta_2 & 0 \end{pmatrix}^{-1} \begin{pmatrix} F_{x,1} \\ M_{\varphi,1} \\ F_{x,2} \end{pmatrix} \tag{1}$$

where k_{xx} is the horizontal translational stiffness, $k_{\phi\phi}$ is the rotational stiffness, $k_{x\phi}$ is the cross-term of k_{mud}, and assuming that k_{mud} is symmetric.

The hysteretic energy loss in each soil element, corresponding to the area of one load-strain cycle (hysteresis loop) is summed over all the whole soil volume to compute a total hysteretic energy loss for the foundation E_h, which is converted with the method described in Carswell et al.[6] into a viscous rotation dashpot value $c_{\phi\phi}$ by

$$c_{\phi\phi} = \frac{E_h}{2\theta^2 \pi^2 f} \tag{2}$$

where θ is the mudline rotation amplitude in rad, f is the loading frequency in Hz, taken here to be the first (fore-aft) natural frequency of the NREL 5MW.

The choice of frequency used for converting the hysteretic foundation damping into a viscous dashpot is based on the assumption that largest contribution to the cyclic moment at mudline is due to vibration at first natural frequency. This assumption likely leads to foundation damping that is overestimated for the frequencies near the selected frequency, while respectively underestimated at frequencies above and beneath the selected frequency. The stiffness and damping characteristics of soil, simultaneously subjected to cyclic loads of different amplitudes, frequencies and directions, is complex [29] and further work is needed to understand this in an OWT design context.

There is no standardized procedure for decomposing foundation damping into different degrees of freedom. While foundation damping is assumed to occur as a function of combined translation and rotation, the difficult of proportioning of converting foundation damping into multiple degrees of freedom is unknown. For the cases analyzed for this particular turbine and foundation, foundation rotation contributes on average 13 times more to the horizontal response at the nacelle than the foundation horizontal displacement, therefore the hysteretic energy loss was modelled with a rotational dashpot to capture this significant influence of the rotational response of the foundation when compared to horizontal displacement.

The elements of k_{mud} and c_{mud} are then used as input to the user defined subroutine *UserPtfmLd* in FAST, which calculates "platform" loads (in this case, loads at the mudline). Perfect fixity was assumed in the vertical z-direction as well as in torsion (rotation about the z-axis, Figure 5).

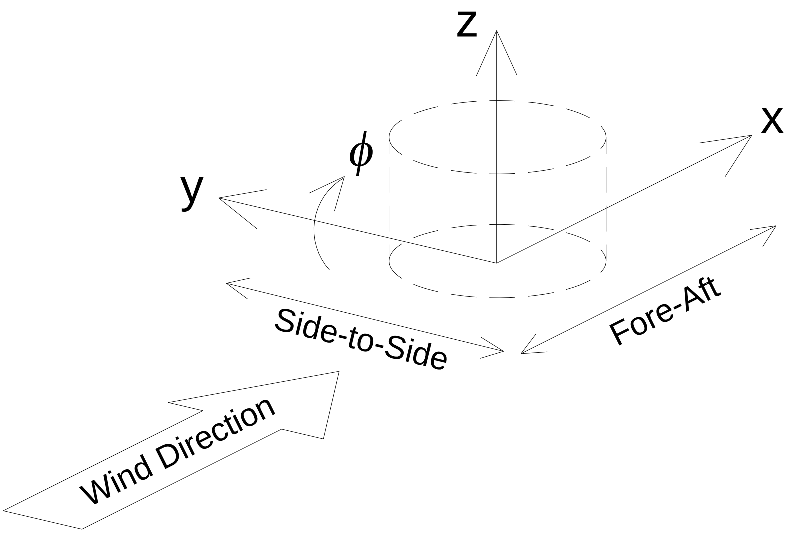

Figure 5 Degrees of freedom in FAST user subroutine

Due to the sign conventions inherent in FAST, the stiffness matrix defined in *UserPtfmLd* is defined as

$$k_{mud} = \begin{pmatrix} k_{xx} & 0 & 0 & 0 & -k_{x\phi} & 0 \\ 0 & k_{xx} & 0 & k_{x\phi} & 0 & 0 \\ 0 & 0 & 0 & 0 & 0 & 0 \\ 0 & k_{x\phi} & 0 & k_{\phi\phi} & 0 & 0 \\ -k_{x\phi} & 0 & 0 & 0 & k_{\phi\phi} & 0 \\ 0 & 0 & 0 & 0 & 0 & 0 \end{pmatrix} \quad \textbf{(3)}$$

Wherein $k_{xx} = k_{yy}$ and $k_{x\phi} = k_{\phi x}$ due to radial symmetry; the mudline damping matrix is defined as

$$c_{mud} = \begin{pmatrix} 0 & 0 & 0 & 0 & 0 & 0 \\ 0 & 0 & 0 & 0 & 0 & 0 \\ 0 & 0 & 0 & 0 & 0 & 0 \\ 0 & 0 & 0 & c_{\phi\phi} & 0 & 0 \\ 0 & 0 & 0 & 0 & c_{\phi\phi} & 0 \\ 0 & 0 & 0 & 0 & 0 & 0 \end{pmatrix}. \quad \textbf{(4)}$$

To reduce the number of analyses we did not define different matrices for the stiffness, k_{mud} and damping c_{mud} for every different yaw angle or wind speed bin within a DLC, rather a representative k_{mud} (and c_{mud}, as applicable) were selected such that individual analysis cases within a DLC could be analyzed using one k_{mud} and therefore also one corresponding compiled version of FAST. FAST has to be recompiled each time one changes the foundation stiffness.

3 NREL 5MW Reference Turbine and Foundation

The NREL 5MW Reference Turbine (NREL 5MW) was used for the analysis, assuming the substructure, foundation, and soil (clay) properties shown in Figure 6 and Table 1. While much of the recently published research focuses on larger turbine models, the NREL 5MW was used in this study because it is more representative of currently installed OWTs. The analysis procedure in this study is similar to the prior study of foundation damping [9] but considers different environmental site parameters. Because metocean data were unavailable for the North Sea site used in this analysis [9,30] (for which the authors had soil information such as undrained shear strength s_u, Poisson's ratio ν, and shear modulus at small strains G_0), metocean data from the Delaware data buoy were used to determine input wave heights and wind speeds for DLC analysis in FAST. The authors believed that using a specific North Sea offshore site was critical because it facilitated comparison with the damping studies performed in literature which are primarily in clayey soils [9,12,13,15,31,32].

Table 1 Structural properties of the NREL 5MW Reference Turbine, substructure, and foundation assuming linearly tapering properties

Location on Support Structure	Diameter, Thickness
Tower top	3.87 m, 0.019 m
Tower base (MSL)	6 m, 0.027 m
Substructure	6 m, 0.10 m
Monopile	6 m, 0.09 m

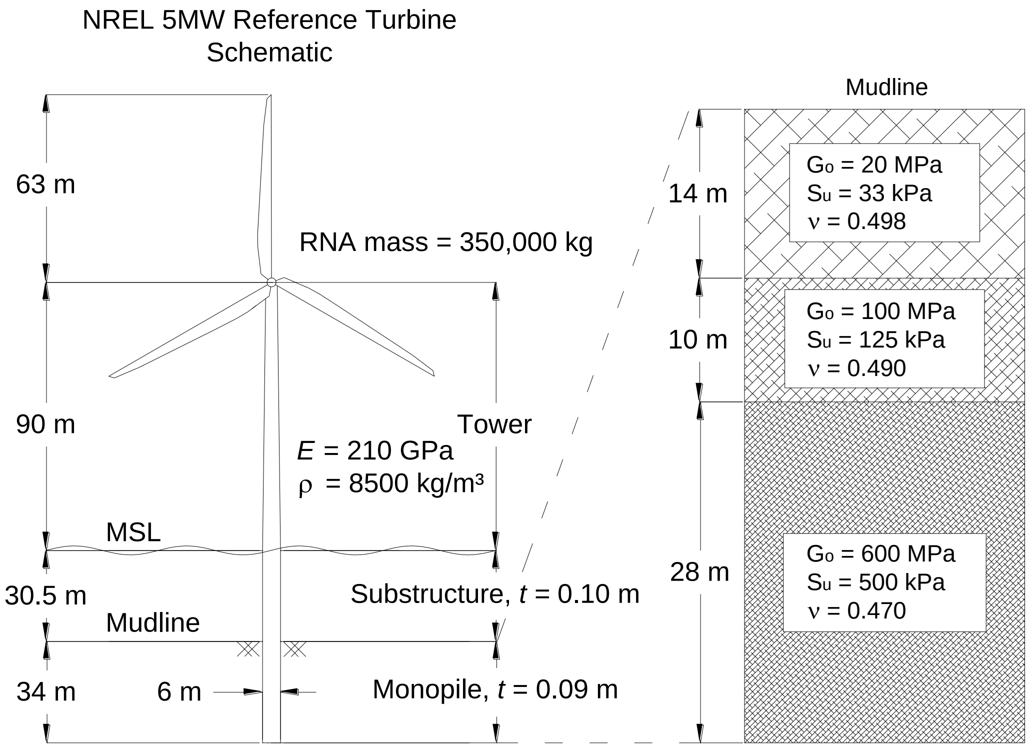

Figure 6 NREL 5MW Reference Turbine Site

4 Offshore Wind Turbine Design Load Cases

The design load cases (DLCs) described in the OWT design standard IEC 61400-3 [18] are used for the vast majority of OWT designs [5,33]. The DLCs for power production, emergency shutdown, and parked conditions (extreme storm loading) were used to assess the effects of foundation damping on the design loads (Table 2). In an effort to reduce the computational expense of the process described in Figure 1, many DLCs were omitted from this study, with scope limited as follows: the fatigue limit state and examination of fatigue life were not considered; due to the higher wind speeds and braking in shutdown DLCs which impact the support structure more, startup DLCs were not considered; normal shutdown DLCs were not included because they do not include wind turbulence (which is considered in emergency shutdown DLCs). Foundation damping is typically much lower than aerodynamic damping for operational OWT conditions [13,34]; therefore, normal power production DLCs are adequate for assessing the influence of foundation damping on the operational OWT system and power production with fault occurrence was excluded. DLCs for transport, assembly, maintenance and repair, were also excluded.

Table 2 IEC offshore wind turbine design load cases analyzed

Design Situation	Load Case	Wind Speed	Wave Height	Yaw Misalignment	Limit State
1) Power production	1.1	NTM $v_{in} < U_{10,hub} < v_{out}$ TI = 11%	NSS $H_s = E[H_s \mid U_{10,hub}]$	0°	ULS
	1.3	ETM $v_{in} < U_{10,hub} < v_{out}$ TI = 16%	NSS $H_s = E[H_s \mid U_{10,hub}]$	0°	ULS
	1.5	EWS $v_{in} < U_{10,hub} < v_{out}$	NSS $E[H_s \mid U_{10,hub}]$	0°	ULS
	1.6a	NTM $v_{in} < U_{10,hub} < v_{out}$ TI = 11%	SSS $H_s = H_{s,50\text{-}yr} \mid U_{10,hub}$	0°	ULS
	1.6b	NTM $v_{in} < U_{10,hub} < v_{out}$ TI = 11%	SWH $H = H_{50\text{-}yr}$	0°	ULS
5) Emergency Shut Down	5.1	NTM v_{rated}, $v_{out} \pm 2$m/s TI = 11%	NSS $E[H_s \mid U_{10,hub}]$	0°	ULS
6) Parked Conditions	6.1a	EWM $U_{hub} = U_{10,50\text{-}yr}$ TI = 11%	ESS $H_s = H_{s,50\text{-}yr}$	± 8°	ULS
	6.1c	RWM $U_{hub} = 1.1U_{10,50\text{-}yr}$	EWH $H = H_{50\text{-}yr}$	± 15°	ULS
	6.2a	EWM $U_{hub} = U_{10,50\text{-}yr}$ TI = 11%	ESS $H_s = H_{s,50\text{-}yr}$	± 180°	ULS Abnormal
	6.2b	EWM $U_{hub} = 1.4U_{10,50\text{-}yr}$	RWH $H = \psi H_{50\text{-}yr}$	± 180°	ULS Abnormal

KEY: NTM = Normal Turbulence Model; ETM = Extreme Turbulence Model; Extreme Wind Shear; RWM = Reduced Wind Model; EWM = Extreme Wind Model; NSS = Normal Sea State; SSS = Severe Sea State; SWH = Severe Wave Height; ESS = Extreme Sea State; EWH = Extreme Wave Height; RWH = Reduced Wave Height; TI = Turbulence Intensity; ULS = Ultimate Limit State; v_{in} = cut-in wind speed; v_{out} = cut-out wind speed; $U_{10,hub}$ = hub height wind speed (10-min average); v_{rated} = rated wind speed; U_{hub} = hub height wind speed; $U_{10,50\text{-}yr}$ = 50-year hub height wind speed (10-min average); H_s = significant wave height; $H_{s,50\text{-}yr}$ = 50-year significant wave height; H = wave height; ψ = wave height reduction factor.

The details of how the DLCs shown in Table 2 were implemented in FAST are described below. Wind-wave misalignment (as studied by Tarp-Johansen et al. [12]) was excluded since it was considered more significant for OWT fatigue life assessment than for foundation ULS design loads; consequently, wind and waves were modeled co-directionally in one direction for all DLCs.

4.1 Power Production

Power production DLCs are relevant for wind speeds within the cut-in and cut-out wind speeds (3 m/s and 25 m/s for the NREL 5MW, respectively); only the rated wind speed (11.4 m/s) and cut-out wind speed (25 m/s) cases were examined in this paper [16].

The ULS DLC 1.4 case was omitted, as we understand that extreme wind direction change primarily tests the OWT controls and not the integrity of the support structure.

Power production DLCs were run in FAST using the simple pitch control and variable speed control provided in the user-defined subroutines. The Thevenin-equivalent, 3-phase induction generator model built into FAST was used.

With the exception of DLC 1.5, all power production DLCs use the Normal Turbulence Model (NTM).

The Extreme Wind Shear (EWS) in DLC 1.5 was used with a steady (non-turbulent) wind input file in FAST, considering only vertical wind shear. FAST does not define horizontal wind shear in the steady wind input files and was thus neglected. Because the steady wind input file is only capable of modeling linear or power law wind shear, the power law wind shear exponent defined for EWS was taken as the average estimated power law exponent over the rotor disk for each second of the 12 second transient EWS event [5].

4.2 Emergency Shutdown

An emergency shutdown occurs when a safety supervisor system turns off the OWT to prevent damage. We model the emergency shutdown with a simplified version of the comprehensive procedure described by [35] as follows:

- The generator was turned off at t = 200 s into the time history simulation.
- Pitch control was overridden at time = 200 s and the blade pitch was set to 90˚ (feathered blades for the NREL 5MW) at the rated limit of 8˚/sec [16].
- The simple high-speed shaft (HSS) brake was then applied 0.6 s after the blade pitch reached 90˚, which is the time it takes the NREL 5MW brake to fully engage after deployment [16].

The emergency shutdown case used the same wind field and wave trains as DLC 1.1.

4.3 Parked Conditions

Several DLCs were omitted from the parked conditions due to similarity:

- DLC 6.2b has the same environmental conditions as DLC 6.1b, but considers loss of electrical connection; DLC 6.1b was omitted, as it was assumed that the loss of electrical connection (blade pitch less than 90˚, ±180˚ yaw misalignment) would cause a more critical load condition.
- DLC 6.3a and 6.3b were similar to DLC 6.2a and 6.2b (respectively), but with a smaller wave height and smaller range of yaw misalignment; DLCs 6.3a and 6.3b were omitted.

The DLCs in the parked condition design situation were all modeled considering parked (i.e, nonrotating) blades. In DLCs 6.1a and 6.1b the blade pitch is 90˚ (feathered blade position), and in DLCs 6.2a and 6.2b the blade pitch is 0˚ due to loss of electrical network connection (and assumedly therefore loss of pitch control).

4.4 Site Specific Environmental Loads

The site specific input to the DLCs are based on the environmental site conditions (summarized in Table 3) taken from the NOAA data buoy 44009 [36] located off the coast of Delaware (DE). The DE buoy data include the 1-hr average wind speed at 5 m above sea level and 1-hr average significant wave height H_s from 1986-2014. Wind speed at hub height was calculated using the power law for vertical wind shear, with an exponent of 0.14 per DNV [5].

Table 3 Wave height and wind speed at particular mean return periods for the Delaware data buoy site used for parked design situation

Site Condition	Value
5-year Significant Wave Height, $H_{s,5\text{-}yr}$	7.1 m
50-year Significant Wave Height, $H_{s,50\text{-}yr}$	8.1 m
50-year Wind Speed at Hub Height (1-hr average), $U_{1hr,50\text{-}yr}$	37 m/s

Wind speeds and significant wave heights used for the DLCs in the parked design situation were calculated using a Generalized Extreme Value (GEV) distribution fit to the maximum annual wind speed and wave height from 1986-2014. This approach is conservative, as the maximum wind speed and maximum wave height are not necessarily simultaneous. The 5-year significant wave height $H_{s,5\text{-}yr}$ was used in the Reduced Wave Height model (DLC 6.2b) to reduce the 50-year wave height $H_{s,50\text{-}yr}$ by the factor ψ, which is a ratio of $H_{s,5\text{-}yr}/H_{s,50\text{-}yr}$.

Peak spectral period T_p was calculated similarly to Valamanesh et al. [37], where

$$T_p = 1.05\left(11.1\sqrt{\frac{H_s}{g}}\right) \tag{5}$$

where H_s is the significant wave height and g is the acceleration due to gravity.

The sea states in the power production DLCs use significant wave height conditional on 10-min average hub height wind speed ($H_s|U_{10,hub}$). Wind speeds from the DE data buoy were separated into 2 m/s bins ranging from 3 m/s (cut-in wind speed) to 25 m/s (cut-out wind speed), and the expected mean and 50-yr (98th percentile) significant wave heights were calculated as a function of a Weibull probability density function [5] fit to the wave data associated with the wind data within each bin. The mean and 50-yr wave heights conditional on wind speed (Table 4) were used to model Normal Sea State (NSS) and Severe Sea State (SSS), respectively. It was assumed for the purposes of this study that the relationship between 1-hr wind speed (from the DE buoy data) and wave height was similar to 10-minute hub height wind speed ($U_{10,hub}$) and wave height.

Table 4 Significant wave height values conditional on wind speed

Mean Wind Speed, $U_{10,hub}$ (m/s)	**Expected Value Conditional on $U_{10,hub}$**		**50-yr Value Conditional on $U_{10,hub}$**	
	Significant Wave Height, H_s (m)	**Peak Spectral Period, T_p (sec)**	**Significant Wave Height, H_s (m)**	**Peak Spectral Period, T_p (sec)**
4	0.87	3.5	1.8	5.0
6	0.89	3.5	1.9	5.1
8	0.95	3.6	2.0	5.2
10	1.1	3.9	2.1	5.4
12	1.3	4.2	2.4	5.8
14	1.5	4.6	2.8	6.2
16	1.8	5.0	3.2	6.7
18	2.1	5.4	3.6	7.1
20	2.4	5.7	4.1	7.5
22	2.8	6.2	4.9	8.3
24	3.2	6.7	5.7	8.9

The rated wind speed for the NREL 5MW is 11.4 m/s and cut-out is 25 m/s; for power production DLCs, the mean (turbulent) wind speed bins of 12 m/s and 24 m/s (ranging from 11-13 m/s and 23-25 m/s) were used for rated and cut-out conditions.

5 Results and Discussion

5.1 Validation of computed foundation damping

To validate this approach for computing foundation damping, the contribution of foundation damping to the overall OWT system damping was calculated using numerical free vibration analysis and compared with damping values found in the literature. The free vibration analysis was used for numerical purposes (i.e., as a method to determine OWT system damping for various mudline damping conditions) and is not meant to represent a true physical condition or DLC. In the free vibration analysis, a static initial tower top displacement was imposed at hub height in the fore-aft direction and then the support structure was permitted to vibrate freely in conditions with no wind or waves, considering parked blades with a blade pitch of 90˚ (feathered blades). The logarithmic decrement method [6] was then used on the resulting time history using a best-fit of a series of amplitudes. Two free vibration analyses were carried out with the foundation stiffness and damping for each of the representative cases – first including structural damping in the tower property input file (1.0%) and then excluding it (structural damping = 0%).

The foundation damping contribution to the OWT system damping was calculated by taking the difference between these two cases (Table 5) assuming that damping for OWTs can be modeled independently and combined linearly, and that aerodynamic and hydrodynamic damping can be neglected in this case [6,12,13,32]. This approach was used due to the manner in which structural damping is accounted for in FAST, and the sensitivity of the percent critical structural damping to input load level [6,38].

Table 5 Percent critical damping of OWT system for all representative mudline stiffness and damping cases

Foundation Stiffness and Damping from Representative Case	Contribution to Percent Critical OWT System Damping by Foundation Damping [%]	Contribution to Percent Critical System Damping by Structural Damping [%]	Percent Critical Total Damping (Foundation + Structural) [%]
DLC 1.1 v_{rated}	0.28	0.28	0.56
DLC 1.6a v_{out}	0.49	0.30	0.79
DLC 5.1 v_{rated}	0.65	0.31	0.96
DLC 5.1 v_{out}	0.58	0.30	0.88
DLC 6.2a Yaw = 60°	0.64	0.31	0.95
DLC 6.2b Yaw = 0°	0.65	0.32	0.97

The foundation damping calculated here (ranging from 0.28% to 0.65%) is within the range found in the literature [6,12,13,15,31,32]. Most notably, the contribution by foundation damping to the percent critical damping of OWT system calculated for emergency shutdown cases (0.58%) is very similar (also 0.58%) to the foundation damping contribution to the OWT system damping estimated by Damgaard et al. [32] from a field rotor-stop test of a wind turbine located at a site with a soil profile dominated by very stiff to very hard clay similar to the one analyzed in this paper. These results offer at least one instance of experimental validation of the approach used in this paper to estimate foundation damping.

The variation in structural damping in Table 5 can likely be attributed to the manner in which structural damping is accounted for in FAST, which is effectively Rayleigh damping with the mass-proportional coefficient set to zero [38]. Consequently, while 1.0% damping was defined in the tower property input file for the first and second fore-aft and side-to-side modes for all DLCs (defining the structural damping for the support structure between mudline and hub height), the net resulting damping attributed to the structure was approximately 0.3%.

5.2 Nonlinear foundation stiffness

The DLCs were grouped based on k_{mud} and E_h, and representative k_{mud} matrices were selected to represent each group (Table 6).

Table 6 Representative mudline stiffness matrices for design load case groups

k_{xx} $\left(\frac{GN}{m}\right)$	$k_{x\phi}$ $\left(\frac{GN}{rad}\right)$	$k_{\phi\phi}$ $\left(\frac{GNm}{rad}\right)$	Decoupling Length (m)	Natural Freq. (Hz)	$c_{\phi\phi}$ $\left(\frac{GNs}{rad}\right)$	Design Load Cases
2.6	20	270	7.7	0.23	2.3	1.1, 1.5, 6.1c
2.6	22	290	8.5	0.23	3.7	1.3, 1.6a, 1.6b
3.3	32	400	9.7	0.23	3.4	5.1 (v_{rated})
3.0	28	350	9.3	0.23	3.5	5.1 (v_{out})
2.8	26	340	9.3	0.23	4.0	6.1a, 6.2a
2.6	24	310	9.2	0.23	4.6	6.2b

The values of k_{xx}, $k_{x\phi}$, and $k_{\phi\phi}$ in the mudline stiffness matrices using the method from Zaaijer [28] above show a counter-intuitive trend: the stiffness values appear to increase with loading conditions (F_x, M_ϕ); however, despite the increase in individual stiffness matrix values, the resulting foundation response (u, θ) and frequency trend appropriately – i.e., with increasing moment amplitude, displacement and rotation increase and frequency decreases, representing a softening in soil-pile response. Prior work on foundation damping by Carswell et al. [9] utilized horizontal and rotational springs at the end of a rigid decoupling length to decouple the 2x2 stiffness matrix model of soil-foundation interaction. Using the rotational spring stiffness as defined by Carswell et al. [9], Figure 7 shows that the rotational stiffness of the soil-pile system decreases with increasing moment as expected, even though the magnitude of individual components of the stiffness matrix may increase. The depth down to so called decoupling point, the horizontal and moment increases with decreasing soil stiffness due to increasing moment amplitude, which is in agreement with other results for monopiles from NGI [39]. The increase in decoupling length with increasing load amplitude causes the mudline rotational stiffness values (given in Table 6) to increase with loading for some of the DLC groups.

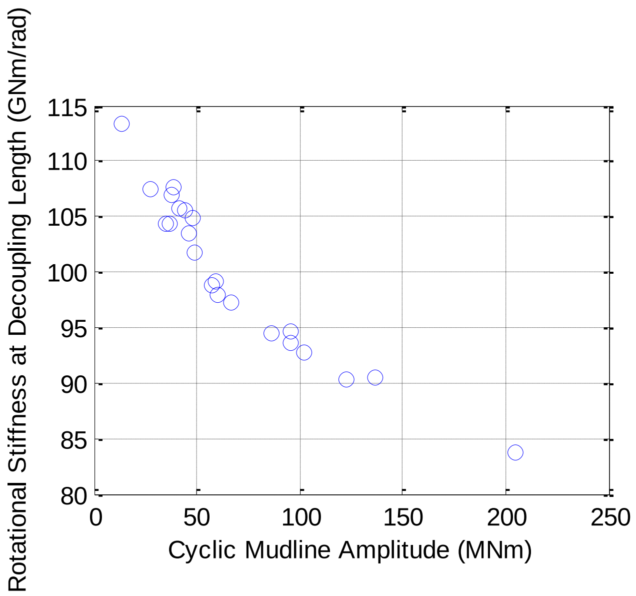

Figure 7 Rotational stiffness at the end of a rigid decoupling length vs. mudline moment

5.3 Response with and without foundation damping

Using the representative mudline stiffness matrices from Table 6, aero-hydro-elastic analyses were performed in FAST including foundation damping ("damped", Table 7) and considering no foundation damping ("undamped"). Cyclic amplitudes for mudline loads, displacements, and rotations decreased for all DLCs when mudline foundation damping was included in the analysis. Broadly speaking, mudline moment amplitude (M_{ϕ},) was reduced more than mudline horizontal force amplitude (F_x) with the inclusion of foundation damping, which is similar to the results found by Carswell et al. [6] (Figure 8).

Table 7 Mudline response comparison between the damped and undamped analyses in FAST. Damped analyses included mudline foundation damping in the form of a viscous rotational dashpot.

Load Case	***Condition***	**UNDAMPED**				**DAMPED**			
		F_x (MN)	M_ϕ (MNm)	u_x (mm)	θ_ϕ (10^{-3} rad)	F_x (MN)	M_ϕ (MNm)	u_x (mm)	θ_ϕ (10^{-3} rad)
1.1	v_{rated}	0.59	42	3.5	0.41	0.57	41	3.4	0.41
	v_{out}	1.3	44	4.3	0.48	1.2	43	4.2	0.47
1.3	v_{rated}	0.66	46	4.5	0.50	0.61	46	4.4	0.49
	v_{out}	1.4	53	5.7	0.61	1.3	51	5.5	0.59
1.5	v_{rated}	0.47	17	1.6	0.19	0.46	17	1.6	0.18
	v_{out}	1.2	34	3.6	0.40	1.2	34	3.6	0.40
1.6a	v_{rated}	0.98	46	4.8	0.52	0.96	45	4.7	0.51
	v_{out}	2.1	56	6.8	0.71	2.1	55	6.7	0.69
1.6b	v_{rated}	1.4	52	5.8	0.61	1.4	51	5.7	0.61
	v_{out}	2.9	65	8.6	0.87	2.9	64	8.5	0.86
5.1	v_{rated}	0.87	88	11	1.1	0.57	56	7.3	0.73
	v_{out}	1.0	72	8.4	0.88	0.91	52	6.3	0.65
6.1a	Yaw = 0°	2.9	98	13	1.3	2.8	81	11	1.1
	Yaw = 8°	2.9	99	13	2.3	2.8	83	12	1.1
6.1c	Yaw = 0°	1.8	38	5.7	0.55	1.8	37	5.6	0.54
	Yaw = 15°	1.8	37	5.6	0.54	1.8	36	5.5	0.53
6.2a	Yaw = 0°	2.9	87	12	1.2	2.9	85	12	1.2
	Yaw = 60°	2.8	100	12	1.2	2.8	82	11	1.1
	Yaw = 90°	3.0	130	16	1.6	2.8	90	11	1.1
6.2b	Yaw = 0°	3.3	61	9.6	0.92	3.3	61	9.5	0.91
	Yaw = 90°	3.3	70	10	0.99	3.3	63	9.7	0.93
	Yaw = 180°	3.4	64	9.9	0.95	3.3	63	9.8	0.94

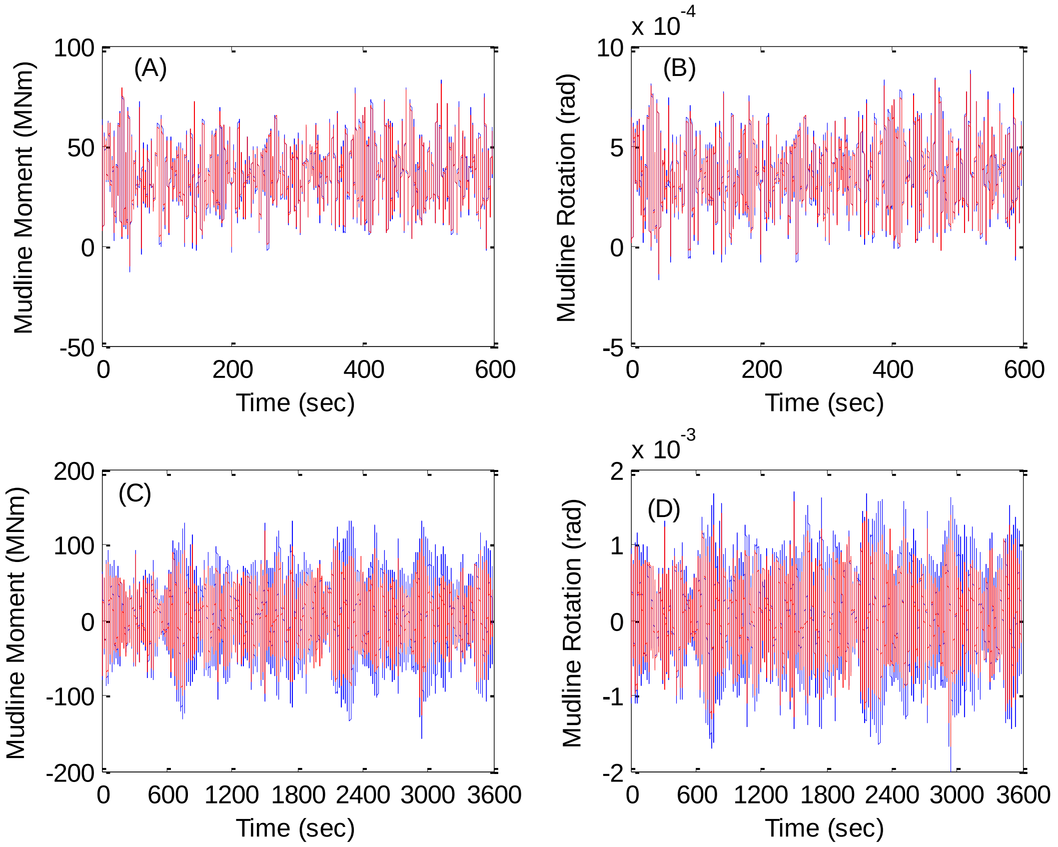

Figure 8 Example time histories of undamped (blue) vs. damped (red). (A) and (B) show mudline moment and rotation for DLC 1.1 at cut-out wind speed; (C) and (D) show mudline moment and rotation for DLC 6.2a at Yaw = 90°. The OWT is in a power-production state for DLC 1.1 (with spinning rotor blades) and parked for DLC 6.2a.

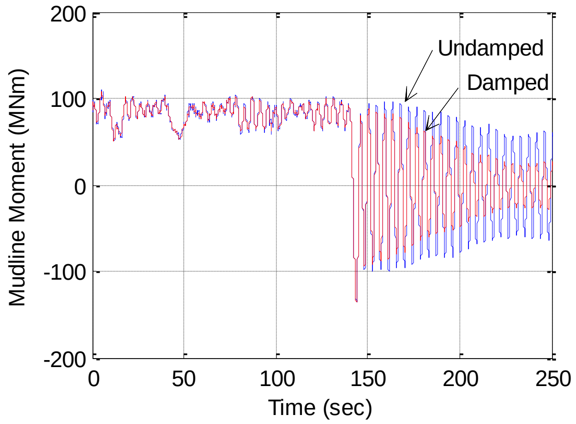

Figure 9 Example time history of undamped vs. damped response for emergency shutdown DLC 5.1 at rated wind speed

Table 8 Percent reduction in mudline response (horizontal mudline shear, moment, displacement and rotation) due to of foundation damping considering Power Production, Emergency Shutdown, and Parked DLC conditions

Design Situation	Load Case	Condition	F_x [%]	M_ϕ [%]	u_x [%]	θ_ϕ [%]
1) Power Production	1.1	v_{rated}	4.1	1.1	1.5	1.3
		v_{out}	2.7	1.8	2.2	2.0
	1.3	v_{rated}	8.2	1.6	2.4	2.1
		v_{out}	7.3	3.3	4.5	4.2
	1.5	v_{rated}	1.7	2.8	2.8	2.7
		v_{out}	0.4	0.8	0.7	0.8
	1.6a	v_{rated}	2.2	1.1	1.5	1.4
		v_{out}	1.4	1.8	1.8	1.8
	1.6b	v_{rated}	1.0	0.6	0.8	0.8
		v_{out}	0.6	0.9	0.9	0.9
	Average		3.0	1.6	1.9	1.8
5) Emergency Shutdown	5.1	v_{rated}	34	36	36	36
		v_{out}	15	30	29	29
	Average		25	33	32	33
6) Parked Conditions	6.1a	Yaw = 0°	1.9	17	12	13
		Yaw = 8°	2.0	17	12	13
	6.1c	Yaw = 0°	1.9	2.8	2.6	2.6
		Yaw = 15°	2.0	1.5	1.4	1.4
	6.2a	Yaw = 0°	0.8	2.3	1.9	2.0
		Yaw = 60°	2.1	19	6.6	9.2
		Yaw = 90°	4.4	30	28	30
	6.2b	Yaw = 0°	0.1	1.1	0.5	0.6
		Yaw = 90°	0.5	9.2	4.6	5.5
		Yaw = 180°	0.8	1.6	1.3	1.4
	Average		1.6	10	7.1	7.9

The emergency shutdown case (DLC 5.1, defined in Section 4.4) displayed the most significant reduction in cyclic mudline demand when foundation damping was included in the analysis (Table 8, Figure 9). The peak response at shutdown is reduced by approximately 5-10%, however, using two times the standard deviation (2σ) of the post-shutdown response (i.e., after t = 140 s in Figure 9) as a comparative metric, the reduction in mudline load and response amplitude after emergency shutdown due to foundation damping is approximately 25-33%. Furthermore, the number of load cycles applied to the foundation reduces by approximately 30%. Using the maximum amplitude in the beginning of the shutdown process (chosen as a simple approach to obtain a first order estimate of the importance of foundation damping for this DLC) likely overestimates the foundation damping for subsequent load cycles; however, accounting for foundation damping the combined reduction in load amplitude and number of cycles could lead to a considerable reduced demand on the foundation, since smaller amplitude load cycles subsequent to large amplitude load cycles may control the foundation capacity [24]. Power production cases were not as significantly affected by foundation damping as emergency shutdown and the parked cases were (Table 8, Figure 8). With the exception of approximately 8% reduction in F_x and 2-5% reduction in u_x and q_ϕ for DLC 1.3, the majority of the reductions in F_x and M_ϕ for power production cases ranged from approximately 1-4% and for u_x and θ_ϕ the reductions were approximately 1-2%.

The parked DLCs showed larger reduction in mudline response compared to the power production cases for which the aerodynamic damping is much more significant than foundation damping [13,34].

The reductions in response are much greater for the turbulent wind, irregular wave cases (DLCs 6.1a and 6.2a) than the steady wind, regular wave cases (DLCs 6.1c and 6.2b): the largest reduction in M_ϕ for the steady wind/regular wave cases was 9.2% (DLC 6.2b, 90˚ yaw case) while for the turbulent wind/irregular wave cases, the largest reduction in M_ϕ was nearly 30% (DLC 6.2a, 90˚ yaw case). The difference in reduction is likely due in part to the larger mudline cyclic amplitude for the turbulent wind/irregular wave cases used to determine mudline foundation damping (for which M_ϕ are on average approximately twice that of the steady wind/regular wave cases), but may also underscore the importance of including foundation damping in stochastic analyses (note that while the components of the stiffness matrices for DLCs 6.2a and 6.2b differ by less than or equal to 10%, the dashpot value $\boldsymbol{c_{\phi\phi}}$ is actually higher for DLC 6.2b than for DLC 6.2a).

6 Summary and Conclusions

This paper analyzed the influence of foundation damping on the behavior of a monopile-supported offshore wind turbine (OWT) considering the design situations of power production, emergency shutdown, and parked conditions. These design situations were modeled in FAST [17] according to the design standard IEC 61400-3 [18], considering the NREL 5MW Reference Turbine [16] and the soil conditions of a site in the North Sea. Because metocean data was unavailable at the North Sea Site analyzed in this paper, environmental conditions from a data buoy in the U.S. Atlantic Ocean were used to determine input wave heights and wind speeds for analysis in FAST.

Foundation damping was modeled using viscous rotational dashpots at the mudline. The dashpot coefficient was calculated as a function of hysteretic energy loss from the soil-pile system and mudline rotation amplitude using the NGI-developed program INFIDEL [19,20] and the first fore-aft natural frequency of the NREL 5MW. The rotational dashpots were used in conjunction with a mudline foundation stiffness matrix to model soil-monopile interaction for the OWT modeled in FAST.

Foundation damping played a more significant role in the emergency shutdown and parked design conditions than power production. For power production cases, the average reduction in cyclic demand (amplitude of mudline loads) due to the inclusion of foundation damping was approximately 3% for horizontal mudline force and 1.6% for mudline moment. Comparatively, the cyclic moment demand was reduced by 10% on average for the parked conditions and by as much as 30% in some cases. The emergency shutdown cases experienced the largest reduction in cyclic mudline demand (25-33%). In all cases, the selection of cyclic load amplitude influences foundation damping results: larger cyclic load amplitudes lead to lower foundation stiffness and more foundation damping and vice versa (Table 6, Figure 7).

The percent critical damping of the OWT system in the free vibration study range was 0.3-0.7% and were in good agreement with those found in literature [6,12,13,15,31,32], particularly with the experimentally-derived estimate of foundation damping from an instrumented emergency shutdown test of an OWT in similar clay soil from Damgaard et al. [32] This validates the general approach used hereinto compute and incorporate foundation damping in an OWT analysis and demonstrates the benefits of including foundation damping into time history analysis. While this paper focused on a specific example, the principles illustrated in this paper are generally applicable to OWTs supported by monopile foundations and it can be expected that similar reductions in cyclic amplitude may be seen in other cases (as the required stiffness of the foundation to meet natural frequency and fatigue criteria would likely result in foundations of similar stiffness).

It may be concluded from this paper that the role of foundation damping in parked and emergency shutdown conditions is significant. For power production cases, the assumption that the first natural frequency is the dominant frequency of the cyclic response may not be accurate, and that in some instances the frequency dominating the cyclic response may be peak wave frequency; consequently, in that instance using the dominant wave frequency in the formulation for foundation damping may increase the accuracy and significance of foundation damping under power production design situations. Additionally, further research on the significance of foundation damping during situations of wind-wave misalignment [12] would also show an increase in the significance of foundation damping during power production design situations.

Future work on foundation damping and fatigue analysis should be performed to better understand how foundation damping influences OWT support structure design: the steel of the support structure may benefit from low amplitude cycle reduction (due to the large number of low amplitude cycles experienced throughout the life of the turbine) while the pile-soil interaction may benefit from high amplitude cycle reduction. Additionally, using harmonic assumptions in the formation of mudline foundation stiffness and damping for highly stochastic time histories does not capture the full complexity of the dynamic behavior of these systems; to better understand the influence of this assumption, a foundation model which can re-calculate mudline foundation stiffness and damping at each load step is required.

The influence of soil profile on foundation damping should be investigated in future work, particularly with regard to soil type – the majority of existing work on foundation damping has focused on clayey soils, with limited information regarding how much damping may be contributed by a monopile in sand and how it may be compared to the amount of damping from clays [6].

There is a need for design guidelines on how to quantify and account for foundation damping in modelling. Current design often includes foundation damping as an increase in overall damping;

however, if foundation damping is accounted for by either a dashpot at the mudline or a macro element approach, the contribution of foundation damping should not also be included in the overall structural damping.

Acknowledgements

The research was supported by the grants CMMI-1234560, CMMI-1234656, the Massachusetts Clean Energy Center and the NSF-sponsored IGERT: Offshore Wind Energy Engineering, Environmental Science, and Policy (Grant Number 1068864), and the Norwegian Geotechnical Institute. Acknowledgement to the project Reducing Cost of Offshore Wind by Integrated Structural and Geotechnical Design (REDWIN), Grant No. 243984.

References

[1] Hamilton B, Battenberg L, Bielecki M, Bloch C, Decker T, Frantzis L, et al. Offshore Wind Market and Economic Analysis: Annual Market Assessment. Burlington, MA: Navigant Consulting, Inc.; 2013.

[2] Clean Energy Pipeline. Offshore Wind Energy: Project Cost Outlook 2014:1–20.

[3] Mone C, Hand M, Bolinger M, Rand J, Heimiller D, Ho J, et al. 2015 Cost of Wind Energy Review 2017.

[4] Wang X, Zeng X, Li X, Li J. Investigation on offshore wind turbine with an innovative hybrid monopile foundation: An experimental based study. Renew Energy 2019;132:129–41. doi:10.1016/j.renene.2018.07.127.

[5] DNV. DNV-OS-J101 Design of Offshore Wind Turbine Structures. Det Norske Veritas AS; 2013.

[6] Carswell W, Johansson J, Løvholt F, Arwade SR, Madshus C, DeGroot DJ, et al. Foundation damping and the dynamics of offshore wind turbine monopiles. Renew Energy 2015;80:724–36. doi:10.1016/j.renene.2015.02.058.

[7] Velarde J, Kramhøft C. Uncertainty Modeling and Fatigue Reliability Assessment of Concrete Gravity Based Foundation for Offshore Wind Turbines 2018:256–64.

[8] Krathe VL, Kaynia AM. Implementation of a non-linear foundation model for soil-structure interaction analysis of offshore wind turbines in FAST. Wind Energy 2017;20:695–712. doi:10.1002/we.2031.

[9] Carswell W, Johansson J, Løvholt F, Arwade SR, Madshus C, DeGroot DJ, et al. Foundation damping and the dynamics of offshore wind turbine monopiles. Renew Energy 2015;80. doi:10.1016/j.renene.2015.02.058.

[10] Skau KS, Kaynia AM, Page AM, Løvholt F, Norén-Cosgriff K, Sturm H, et al. REDWIN – REDucing cost in offshore WINd by intregrated structural and geotechnical design. Geteoteknikkdagen 2017:38.1-38.17.

[11] GL WindEnergie. Overall Damping for Piled Offshore Support Structures, Guideline for the Certification of Offshore Wind Turbines. Germanischer Lloyd WindEnergie; 2005.

[12] Tarp-Johansen NJ, Andersen L, Christensen E, Mørch C, Kallesøe B, Frandsen S. Comparing Sources of Damping of Cross-Wind Motion. Eur. Offshore Wind 2009 Conf. Exhib. 14-16 Sept., Stockholm, Sweden: European Wind Energy Association; 2009.

[13] Shirzadeh R, Devriendt C, Bidakhvidi M a., Guillaume P. Experimental and computational damping estimation of an offshore wind turbine on a monopile foundation. J Wind Eng Ind Aerodyn 2013;120:96–106. doi:10.1016/j.jweia.2013.07.004.

[14] Wind Europe. The European offshore wind industry: Key trends and statistics 2016. 2017.

[15] Damgaard M, Andersen J, LB I, Andersen L. Time-Varying Dynamic Properties of Offshore Wind Turbines Evaluated by Modal Testing. Proc. 18th Int. Conf. Soil Mech. Geotech. Eng., Paris: 2013, p. 2343–6.

[16] Jonkman J, Butterfield S, Musial W, Scott G. Definition of a 5-MW Reference Wind Turbine for Offshore System Development. 2009.

[17] Jonkman J, Buhl MJ. FAST User's Guide. Golden, CO: National Renewable Energy Laboratory; 2005.

[18] IEC 61400-3. Design Requirements for Offshore Wind Turbines. Brussels: 2009.

[19] NGI. Description of INFIDEL - a non-linear, 3-D finite element program. 1991.

[20] Hansteen OE, Höeg K. Soil-Structure Interaction Analysis of Embedded Caisson Anchor Under Tension Load. BOSS '94, 7th Int. Conf. Behav. Offshore Struct., Cambridge, MA: 1994, p. 49–62.

[21] Bir GS. User's Guide to BModes (Software for Computing Rotating Beam Coupled Modes). Golden, CO: 2007.

[22] Skau KS, Torgersrud Ø, Jostad HP, Hofstede H, Hermans S. Linear and nonlinear foundation response in dynamic analyses of jack-up structures. Front Offshore Geotech III 2015:978–1.

[23] Andersen KH. Bearing capacity under cyclic loading — offshore, along the coast, and on land. The 21st Bjerrum Lecture presented in Oslo, 23 November 2007. Can Geotech J 2009;46:513–35. doi:10.1139/T09-003.

[24] Sturm H. Design Aspects of Suction Caissons for Offshore Wind Turbine Foundations. In: Shin Y, editor. Proc. ISSMGE TC 209 Work., Seoul, Korea: 2017.

[25] Løvholt F, Madshus C, Andersen KH. Intrinsic soil damping from cyclic laboratory tests with average strain development. ASTM Geotech Test J n.d.

[26] Norén-cosgriff K, Jostad HP, Madshus C. Idealized load composition for determination of cyclic undrained degradation of soils. In: Meyer V, editor. Front. Offshore Geotech. III, London: Taylor & Francis Group; 2015, p. 1097–102.

[27] Darendeli M. Development of a new family of normalized modulus reduction and material damping curves. Austin, TX: University of Texas at Austin; 2001.

[28] Zaaijer MB. Foundation modelling to assess dynamic behaviour of offshore wind turbines. Appl Ocean Res 2006;28:45–57. doi:10.1016/j.apor.2006.03.004.

[29] Madshus C. Soil Non-linearity and its Effect on the Dynamic Behaviour of Offshore Platform Foundations. University of Oslo, 1997.

[30] Hamre L, Khankandi SF, Strøm PJ, Athanasiu C. Lateral behaviour of large diameter monopiles at Sheringham Shoal Wind Farm. Front. Offshore Geotech. II, 2011, p. 575–80.

[31] Versteijlen W, Metrikine A, Hoving J, Smid E, de Vries W. Estimation of the vibration decrement of an offshore wind turbine support structure caused by its interaction with soil. EWEA Offshore Conf., Amsterdam, the Netherlands: European Wind Energy Association; 2011.

[32] Damgaard M, Andersen J, Ibsen LB, Andersen L. Natural Frequency and Damping Estimation of an Offshore Wind Turbine Structure. Proc. Twenty-second Int. Offshore Polar Eng. Conf.,

vol. 4, Rhodes, Greece: 2012, p. 300–7.

[33] ABS. Offshore Wind Turbine Installations. US Pat App 13/318,316 2010.

[34] Valamanesh V, Myers A. Aerodynamic Damping and Seismic Response of Horizontal Axis Wind Turbine Towers. J Struct Eng 2014;140. doi:10.1061/(ASCE)ST.1943-541X.0001018.

[35] Pedersen AS, Steiniche CS. Safe Operation and Emergency Shutdown of Wind Turbines. Aalborg University, 2012.

[36] NOAA. National Data Buoy Center 2015. http://www.ndbc.noaa.gov/.

[37] Valamanesh V, Myers AT, Arwade SR. Multivariate analysis of extreme metocean conditions for offshore wind turbines. Struct Saf 2015;55:60–9. doi:10.1016/j.strusafe.2015.03.002.

[38] Jonkman B. Natural frequency and damping ratio calculation 2013. https://wind.nrel.gov/forum/wind/viewtopic.php?f=3&t=789 (accessed July 14, 2015).

[39] NGI. Foundation dynamics and effects on OWT behaviour: Effect Of Foundation Stiffness And Damping On The Dynamic Behaviour Of An Offshore Wind Turbine Structure, Report 20140389-01-R, 2016-04-06. 2016.